Legchenko, A., 2007. MRS measurements and inversion in presence of EM noise. *Boletín Geológico y Minero,* 118 (3): 489-508
ISSN: 0366-0176

MRS measurements and inversion in presence of EM noise

A. Legchenko

Institut de Recherche pour le Développement (IRD-LTHE). Mailing address: LTHE, BP53, 38041, GRENOBLE Cedex 9, France.
Tel: +33 4 76 82 50 63. Fax: +33 4 76 82 50 14.
Email: anatoli.legtchenko@hmg.inpg.fr

ABSTRACT

The Magnetic Resonance Sounding method (MRS) is based on the resonance behavior of proton magnetic moments in the geomagnetic field. As the signal generated by the protons is very small, the method is sensitive to electromagnetic noise and this is one of the major limitations for practical application. The frequency of the magnetic resonance signal is directly proportional to the magnitude of the geomagnetic field, and varies between 800 Hz and 2800 Hz around the globe. Whilst natural noise within this frequency range is generally not very large (excepting magnetic storms or other temporary disturbances), the level of cultural noise (electrical power-lines, generators, etc.) may be very high. Both the depth of investigation and resolution of the MRS method depend on signal to noise ratio. If measured data are corrupted by noise, it will have an effect on the accuracy and reliability of MRS results. Consequently, the MRS signal has to be measured with an acceptable signal to noise ratio. For improving the signal to noise ratio different filtering techniques could be applied. Selection of the filtering scheme depends on the noise origin. In any case, application of the stacking is necessary. A large number of repetitive measurements are often required for stacking and consequently one sounding may take from one to twelve hours. In this paper, efficiency of different filtering techniques, inversion strategy and influence of non-filtering noise on MRS results are discussed.

Key words: EM noise, MRS, MRS inversion, MR sounding, power-line harmonics

Medición e inversión de SRM en presencia de ruido EM

RESUMEN

El método de Sondeos de Resonancia Magnética (SRM) se basa en el fenómeno de resonancia de los momentos magnéticos de los protones de hidrógeno en el campo geomagnético. Puesto que la señal generada por los protones es muy pequeña, el método es sensible a la existencia de ruido electromagnético, suponiendo una de sus mayores limitaciones en aplicaciones prácticas. La frecuencia de la señal de resonancia magnética es directamente proporcional a la magnitud del campo geomagnético, y varía entre 800 Hz y 2800 Hz en toda la Tierra. Mientras que, dentro de este rango de frecuencias, los ruidos naturales no son en general de mucha amplitud (excepto los debidos a tormentas magnéticas y otras perturbaciones temporales), el nivel del ruido cultural (líneas eléctricas, generadores, etc.) puede ser muy elevado. Tanto la profundidad de investigación como la resolución de un SRM dependen de la relación entre la señal y el ruido. Si las mediciones están contaminadas por ruido, la exactitud y fiabilidad de los resultados se verán afectadas. En consecuencia, la señal SRM tiene que medirse con una relación señal/ruido aceptable. Para mejorar esta relación pueden utilizarse diversos sistemas de filtrado. Su selección depende del origen del ruido. En cualquier caso, es necesario utilizar métodos de adición de señales, para lo que frecuentemente se requiere un número elevado de repeticiones de la medida, lo que conlleva que la realización de un sondeo pueda durar desde una a doce horas. En este trabajo se presentan la eficacia de diferentes técnicas de filtrado, la estrategia para la inversión y la influencia del ruido en los resultados de un SRM.

Palabras clave: armónicos de líneas eléctricas, inversión SRM, ruido EM, sondeo RM, SRM

Introduction

One of the major limitations of the Magnetic Resonance Sounding method (MRS) is the sensitivity to natural and man-made electromagnetic (EM) noise. Natural EM noise is considered as non correlated noise. It can be created by magnetic storms, telluric currents, thunderstorms etc. Man-made EM noise can be generated by electrical power-lines, electrical generators, radio transmitters, electrical fences, cars and trains, gas pipes with the electrical protection etc. Industrial EM noise is usually considered as a superposition of harmonics of the industrial frequency (50 or 60 Hz). Radio transmitters and telephone lines may also produce man-made EM noise due to different stable frequencies used for the modulation used for communication signals.

An alternating magnetic field produced by the precession of proton magnetic moments in groundwater varies between 10^{-12} and $4x10^{-9}$ T. The voltage created by this magnetic field (MRS signal) varies between 10 nV and 4000 nV when using a wire loop of 100 m

diameter as a receiving antenna and, contrary to many geophysical techniques, the signal cannot be amplified by increasing the transmitter power. The frequency of the magnetic resonance signal (the Larmor frequency) is directly proportional to the magnitude of the geomagnetic field, and varies between 800 Hz and 2800 Hz around the globe. Usually, MRS can be used without major problems within this frequency range because the natural noise is sufficiently low. However, in areas where industrial noise is much stronger than natural noise, power-line harmonics may create a major problem, particularly when the Larmor frequency is close to one of the harmonics of the fundamental frequency (50 Hz or 60 Hz). The noise can be diminished through application of special noise-reducing loops and signal stacking during the field measurements (see Plata and Rubio (2007), and Bernard (2007) in this Issue) and also applying numerical filtering techniques. Depending on field conditions, these procedures can be more or less efficient, but some part of non-filtering noise is always remaining in the records.

MRS provides free water content distribution in the subsurface which is a solution of integral equation and, like many other ill-posed problems, the inversion is sensitive to field measurement errors caused by EM noise. Consequently, MRS results are always suffering from the erroneous data. In some cases errors may be so large that MRS results are getting unreliable.

In this paper attempt was made to summarize nowadays experience of MRS practical application in noisy conditions and to propose an optimal strategy of MRS measurements and interpretation.

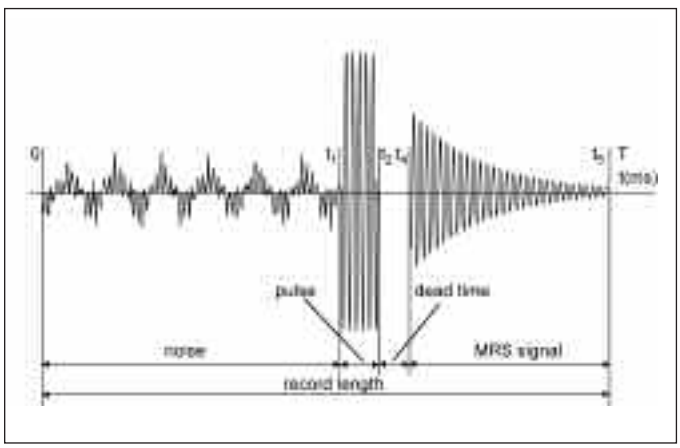

Fig.1. NUMIS record
Fig. 1. Registro NUMIS

NUMIS record

The standard NUMIS MRS equipment developed by IRIS Instruments acquires data in the form of time series recorded before and after the pulse transmission. Each record before the pulse is considered as noise only whereas records after the pulse contain both signal and noise. Before digitizing, a hardware band-pass filter with a ± 100 Hz bandwidth (at the 3 dB level) centered at the excitation pulse frequency is applied. This central frequency is set to equal the Larmor frequency measured by proton magnetometer at each investigated site. The time diagram of the signal measurement process is shown in Figure 1.

For spectral analysis, the time series are digitized with a sampling frequency four times higher than the Larmor frequency $f_s=4f_L$ so as to fully satisfy Shannon's sampling theorem, and to allow full and accurate recovery of both noise and signal passing through the hardware filter. For measuring the signal envelope, a synchronous detector with a low-pass filter of 100 Hz band-pass (at the 3dB level) is applied (Max, 1981). After the synchronous detection, the sampling frequency is set at 500 Hz.

The synchronous detector has two orthogonal channels (X and Y). For both channels, the reference frequency f_{sd} is set as close as possible to the signal frequency, that is the Larmor frequency f_L.The phase of the reference frequency for the X channel coincides with the phase of the current in the loop, and the phase of the frequency for the Y channel is shifted 90 degrees. The amplitude and phase of the signal after the synchronous detector are

$$A(t) = \sqrt{X^2(t) + Y^2(t)}$$

and

$$\Phi(t) = \tan^{-1}(Y(t) / X(t))$$

respectively. In this way, two derived signals are obtained, one in phase and one out of phase:

$$X(t) = E_0 \exp(-t / T_2^*) \cos(\delta\omega \cdot t + \varphi_0) + \sum_k p_k \cos(\delta\omega_k t + \varphi_k) + \varepsilon_x(t) \quad [1]$$

$$Y(t) = E_0 \exp(-t / T_2^*) \sin(\delta\omega \cdot t + \varphi_0) + \sum_k p_k \sin(\delta\omega_k t + \varphi_k) + \varepsilon_Y(t) \quad [2]$$

where $\delta\omega = 2\pi\,\delta f = 2\pi(f_{sd}-f_L)$, p_k, $\delta\omega_k = 2\pi\delta f_k = 2\pi(f_{sd}-$

f_k), and φ_k are the amplitude, the frequency, and phase of the k^{th} power-line harmonic (with K being the number of harmonics passed through the hardware filter); and

$$\varepsilon = \sqrt{\varepsilon_x^2 + \varepsilon_Y^2}$$

is the non-regular noise.

For obtaining E_0 and T_2^* it is assumed that

$$E_0 >> \varepsilon + \sum_k p_k$$

and, thus, the logarithm of the measured amplitude can be calculated, followed by a linear regression fit:

$$\log(A) = \log(E_0) - t / T_2^* + \sum_k p_{Logk}(t) + \varepsilon_{Log}(t) \quad [3]$$

where

$$\sum_k p_{Logk}(t)$$

and

$$\varepsilon_{Log}(t)$$

is the logarithmic noise induced by the noise components X and Y. The phase of the measured signal at time t is composed of the initial phase φ_0 plus the phase shift caused by the frequency offset between the signal frequency and the synchronous detector reference frequency:

$$\Phi(t) = \delta\omega \cdot t + \varphi_0 + \varphi_p(t) + \varphi_\varepsilon(t) \quad [4]$$

where $\varphi_p(t)+\varphi_\varepsilon(t)$ is the phase instability caused by the regular and non-regular noise. A linear regression fit is then applied to determine $\delta\omega$ and hence f_L and φ_0.

The linear regression fit provides a reliable estimate of signal parameters when the noise is low. However, the algorithm is sensitive to noise and, in order to diminish noise influence, a non-linear regression curve-fitting technique based on least squares minimization must be used:

$$\left[\int_{t4}^{t5} (X(t) - X_{mod}(t))^2 dt + \int_{t4}^{t5} (Y(t) - Y_{mod}(t))^2 dt\right] = \min \quad [5]$$

where (t_5-t_4) is the record length (Figure 1),

$$X_{mod}(t) = E_0 \cos(\delta\omega \cdot t + \varphi_0) \exp(-t / T_2^*)$$

and

$$Y_{mod}(t) = E_0 \sin(\delta\omega \cdot t + \varphi_0) \exp(-t / T_2^*)$$

For minimization, the Marquardt non-linear fitting technique (Marquardt, 1963) was used, with the starting point derived from the linear regression estimate presented above (Legchenko and Valla, 1998).

Processing of MRS Signal contaminated by EM noise

We can distinguish four major types of EM noise: natural quasi-constant or time-varying noise, man-made short spikes and industrial noise. Depending on the nature of the EM noise, different strategies of data processing could be applied.

Quasi-constant EM noise

As the proton magnetic resonance response is usually very small in comparison with both cultural and natural electromagnetic noises, even a very narrow filter does not allow getting a good enough signal to noise ratio (S/N). In order to improve the signal to noise ratio a stacking procedure must also be used. It consists of averaging up records:

$$X(t) = \sum_{i=1}^{n} X_i(t) / n$$

and

$$Y(t) = \sum_{i=1}^{n} Y_i(t) / n$$

In case of non-correlated noise the signal to noise ratio is increased $\sqrt{n}$ times after n stacks.

Time-varying EM noise

A more effective stacking scheme, namely weighted stacking, can be applied if the noise magnitude is much larger than the signal and is not statistically constant during data acquisition time (non-white noise). Such a scheme is based on a noise estimate s_i defined as

$$s_i^2 = \frac{1}{\Delta T} \int_0^{\Delta T} (X_i(t)^2 + Y_i(t)^2) dt \quad [6]$$

ΔT being the observation window. Each record is assigned the weight $\eta_i = 1/s_i^2$ and records are averaged up with such weights:

$$X(t) = \sum_{i=1}^{n} \eta_i X_i(t) / \sum_{i=1}^{n} \eta_i$$

and

$$Y(t) = \sum_{i=1}^{n} \eta_i Y_i(t) / \sum_{i=1}^{n} \eta_i \qquad [7]$$

Man-made short spikes

Short spikes appearing with the period of 0.5-2 s is a noise typically generated by electrical fences. If the duration of a spike is smaller than duration of MRS signal then spikes can be efficiently rejected. For that, a spike can be discriminated by its amplitude which is much higher than the signal amplitude (Figure 2a). After spike rejection the signal can be further processed (stacking, filtering).

Industrial electromagnetic noise

A special field study was undertaken in order to learn more about industrial EM noise (Legchenko and Valla, 2003). The frequency range of interest for the MRS method is between 800 Hz and 2800 Hz, which corresponds to worldwide variations of the Larmor frequency set by the Earth's magnetic field. The study was carried out mainly in areas with the Larmor frequency around 2000 Hz, but it is likely that this does not change the general nature of the results. The field data were recorded in France and also in other countries; field data in this paper were acquired at three sites in France, one in Israel, one in the Netherlands and one in the USA.

A first appraisal of noise can be made by computing its RMS amplitude as

$$\eta = \frac{1}{N} \cdot \sum_{i=1}^{N} \sqrt{X_i^2 + Y_i^2} \qquad [8]$$

where N is the number of samples in a noise record after the synchronous detector. An example of noise measurements in France is shown in Figure 3. At each site, 40 consecutive 1000 ms long records of the noise were made, at about ten-second intervals. The sampling rate was 2 ms which makes N=500 in Equation 8. It can be seen that even at the same test-site the noise magnitude was not stable and may vary by a factor of more than two.

A more detailed analysis was made using the Fourier transform. Figure 4 shows the Fourier spectra of noise records at four different test sites. Industrial frequency harmonics dominate in all the spectra. However, the amplitudes of even and odd harmonics and the non-harmonic noise vary significantly from one site to another. Note that, as the records from the USA are for relatively short time periods (200 ms instead of 1000 ms), the bandwidth of power-line harmonics in the USA spectrum appears correspondingly wider.

Industrial frequency stability is the keystone of the power-line noise filtering techniques proposed by Butler and Russell (1993). In 1993 and later (Butler,

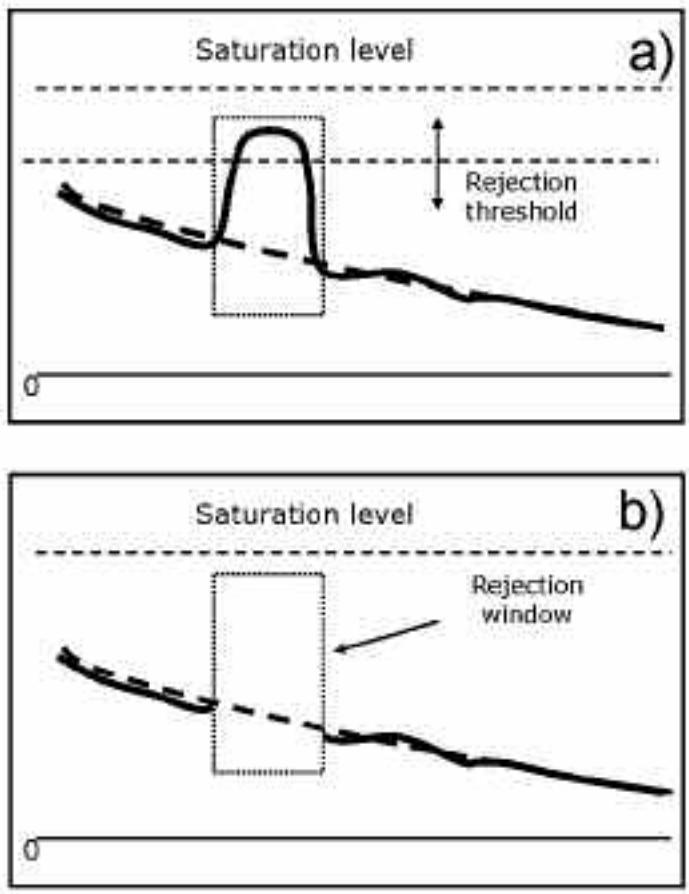

Fig. 2. Short spikes rejection scheme (solid line – signal with spike, thick dashed line – signal without spike). a) before rejection, b) after rejection

Fig. 2. Esquema del sistema de rechazo de picos de ruido (línea gruesa continua - señal con ruido, línea gruesa discontinua- señal sin ruido). a) antes del rechazo, b) después del rechazo

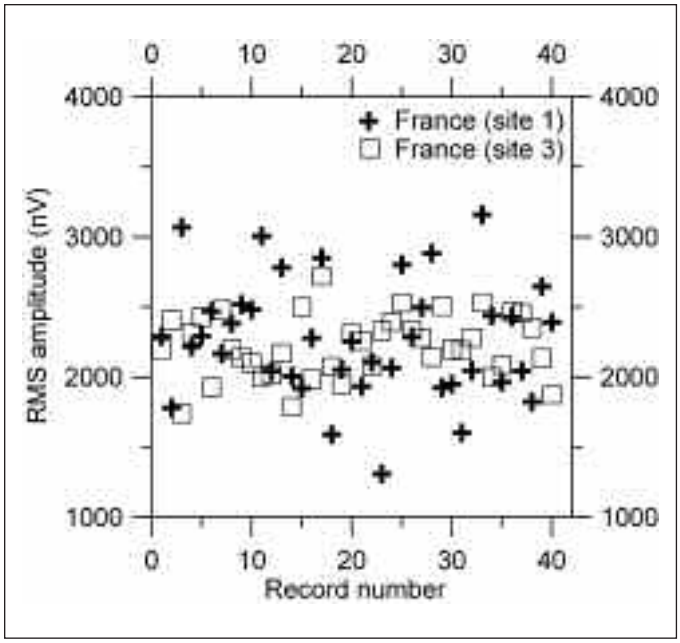

Fig. 3. Example of variations in the magnitude of power-line noise
Fig. 3. Ejemplo de variaciones en la magnitud del ruido producido por líneas eléctricas

2001), the authors showed the consequences of incorrect frequency estimation on the performance of subtraction schemes. In order to check the stability assumption, measurements were made of power-line harmonic frequencies in the investigated frequency range (37th harmonic in Israel, 40th in France, and 41st in the Netherlands) using the synchronous detector described above. It can be seen (Figure 5) that frequencies vary from one record to another, but the instability is site-dependent with the largest variations being observed in Israel. Such considerable instability of an industrial frequency is, in fact, very unusual and there is no clear reason why it occurs. However, even in the same country (France, Sites 1 and 2) the frequency estimates show some instability. This instability (variations around 0.5 Hz and even higher) can be explained partly by instability of the power-line fundamental frequency, and partly by noise influencing the accuracy of the estimation.

The proportion of 50 Hz harmonics in the noise spectra was also calculated (Figure 6). In order to diminish the spectral leakage effect caused by limited resolution of the Fourier transform on the accuracy of

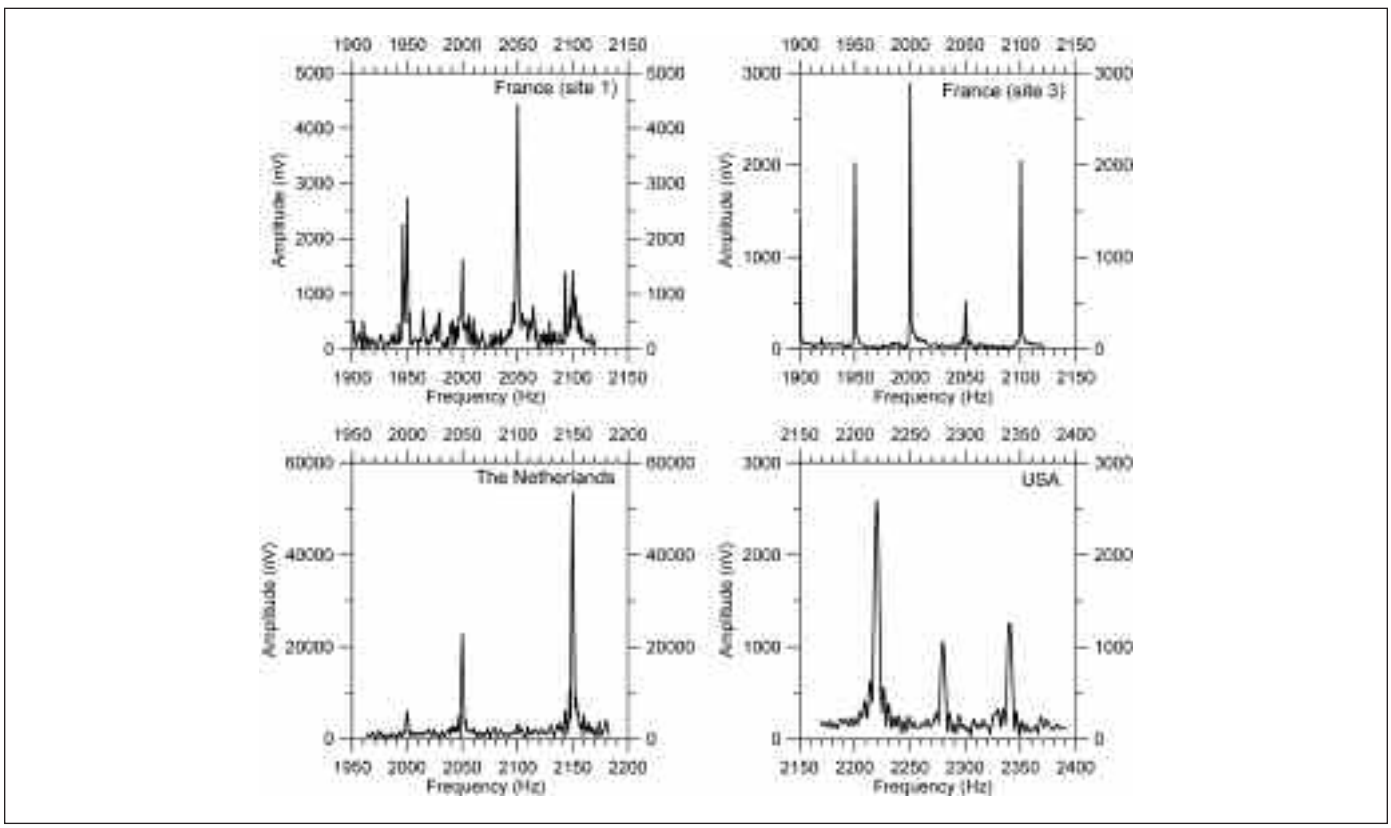

Fig. 4. Examples of power-line spectra
Fig. 4. Ejemplos del espectro del ruido producido por líneas eléctricas

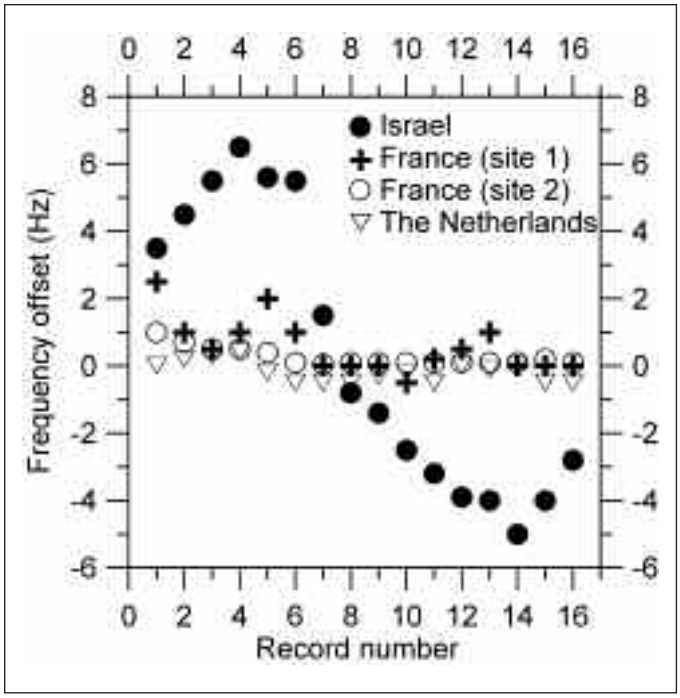

Fig. 5. Example of measurements of the frequency of kth power-line harmonic relatively its 50 kHz estimate at different sites
Fig. 5. Ejemplo de las frecuencias medidas de los armónicos de una línea eléctrica (valores relativos a 50 kHz) en distintos sitios

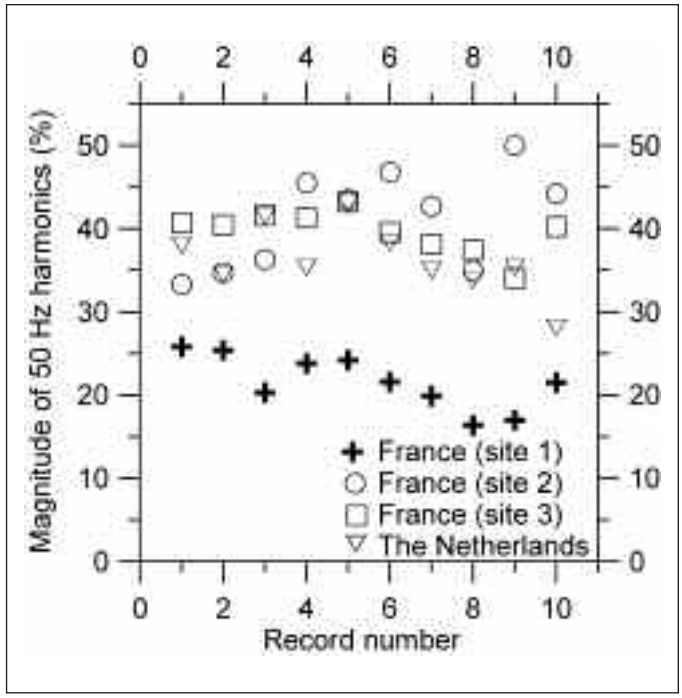

Fig. 6. Proportion of 50 Hz harmonics in the total noise
Fig. 6. Proporción de la contribución de los armónicos de 50 Hz al ruido total

the estimation, the ±1 Hz bandwidth around each harmonic was taken into account for the calculations. It was found that, depending on the site, the power-line harmonics represent only 20% to 50% of the noise energy within the ±150 Hz bandwidth. This high percentage of non-stationary noise observed in the vicinity of power-lines may be explained by the fact that in the investigated frequency range the most energetic (and probably more stable) lower harmonics are filtered out and only the higher harmonic numbers (20 to 55) are used. It is also possible that power-lines, being long conductors, act as electromagnetic antennae and channel both man-made and natural electromagnetic noises from a large area, thus amplifying the grossly random background noise, especially on the vertical magnetic component that is measured with MRS antennae.

Industrial EM noise can be efficiently diminished by applying the noise reducing field setup composed of two circles or squares that form the figure eight (Trushkin *et al.,* 1994). Depending on site conditions, the figure-eight-loop allows improving the S/N from two to ten folds. However, even with this loop the S/N may be not sufficiently good for inversion.

Filtering technique: block subtraction

After the synchronous detector and low-pass filter, only three power-line harmonics around the Larmor frequency can be considered harmful for MRS signal measurement: $f_{k-1}=\Delta F-50$, $f_k=\Delta F$, and $f_{k+1}=\Delta F+50$; where $\Delta F=(50k-f_{sd})$, $f_{sd}\approx f_L$ and k is closest to the Larmor frequency power-line harmonic.

For practical implementation of the block subtraction method, it is assumed that the noise is regular and largely dominant over the signal (otherwise, filtering would not be needed) and, therefore, that non-stacked signal records are mostly noise. The block subtraction method for such a case is shown in Figure 7. The strategy consists of selecting the time shift τ so that the noise sample B(t) from a noise record, and the sample A(t) that contains both signal and noise, are as similar as possible. An ideal sample rate would be an integer multiple of 50 Hz. However, the finite sample interval of the record and uncertainty over the exact value of the fundamental frequency limits the accuracy of the subtraction in this case. In order to diminish errors caused by erroneous estimation of the fundamental frequency, the correlation function

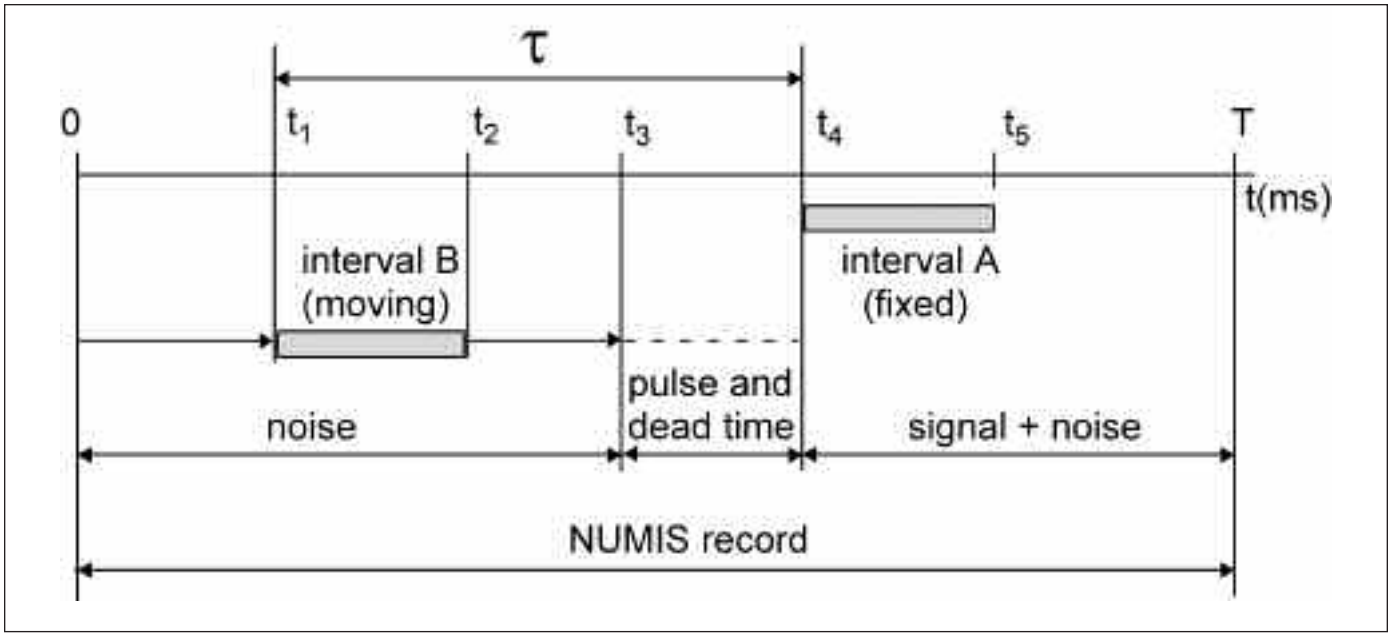

Fig. 7. Selection of the best noise block from a noise record
Fig. 7. Selección del mejor intervalo en un registro del ruido

between a fixed sample A(t) and a moving sample B(t) are used as criteria for the best selection of τ:

$$R_{AB}(t,T)=\left[\frac{\int_{t_4}^{t_5} X_A(t)X_B(t-\tau)dt}{\sqrt{\int_{t_4}^{t_5} X_A^2(t)dt\int_{t_1}^{t_2} X_B^2(t)dt}}+\frac{\int_{t_4}^{t_5} Y_A(t)Y_B(t-\tau)dt}{\sqrt{\int_{t_4}^{t_5} Y_A^2(t)dt\int_{t_1}^{t_2} Y_B^2(t)dt}}\right]=\max \quad [9]$$

where X and Y are the channels of the synchronous detector and $\Delta t=t_2-t_1=t_5-t_4$ (Δt=200 ms for a typical NUMIS setup).

An ideal noise sample would be when $R_{AB}(t,\tau)=2$, but in practice the best value τ_{best} is when $R_{AB}(t,\tau_{best})=\max$. The efficiency of block subtraction can be demonstrated using two different noise records made in France.

In Figure 8, the amplitude of noise sample (A(t)), after processing by the synchronous detector $A(t)=(X^2(t)+Y^2(t))^{1/2}$ is plotted versus time and shown by the thin line. The mean value of the amplitude is given by the 2000 Hz harmonic, but the 1950 Hz and 2050 Hz harmonics are also clearly seen on the plot.

As ΔF=-10 Hz for these sites, the harmonics are presented as a combination of 40 Hz and 60 Hz sinusoids respectively. The results of the subtraction (A(t)-B(t)) is depicted by the thick line. For the record from Site 1, $R_{AB}(t,\tau_{best})=1.4$ and the subtraction is inefficient, whereas for Site 3, $R_{AB}(t,\tau_{best})=1.92$ and the subtraction technique works well. If the proportion of 50 Hz harmonic in the power-line noise recorded at Site 1 (about 20%) is compared with Site 3 (about 40%) (Figure 6), it can be concluded that the block subtraction method gives better results when the percentage of 50 Hz harmonics (regular part) is larger. This conclusion matches exactly that of Butler and Russell (1993) concerning the efficiency of the block subtraction technique for the 0.1-1000 Hz frequency range.

Filtering technique: sinusoid subtraction

The sinusoid subtraction technique is based on the representation of power-line noise as harmonics superimposed on the fundamental frequency (50 Hz or 60 Hz). The harmonic component is estimated from noise records and then subtracted from records containing both the signal and noise. The frequency of power-line harmonics, being relatively unstable, should not be determined by simply multiplying the fundamental frequency value by an integer number. During fieldwork, estimates must be made from the records, not only of the amplitude and phase of a power-line harmonics, but also its frequency.

When applying this technique to MRS signal filtering, it should be kept in mind that the harmonics furthest from the Larmor frequency f_L are filtered out by

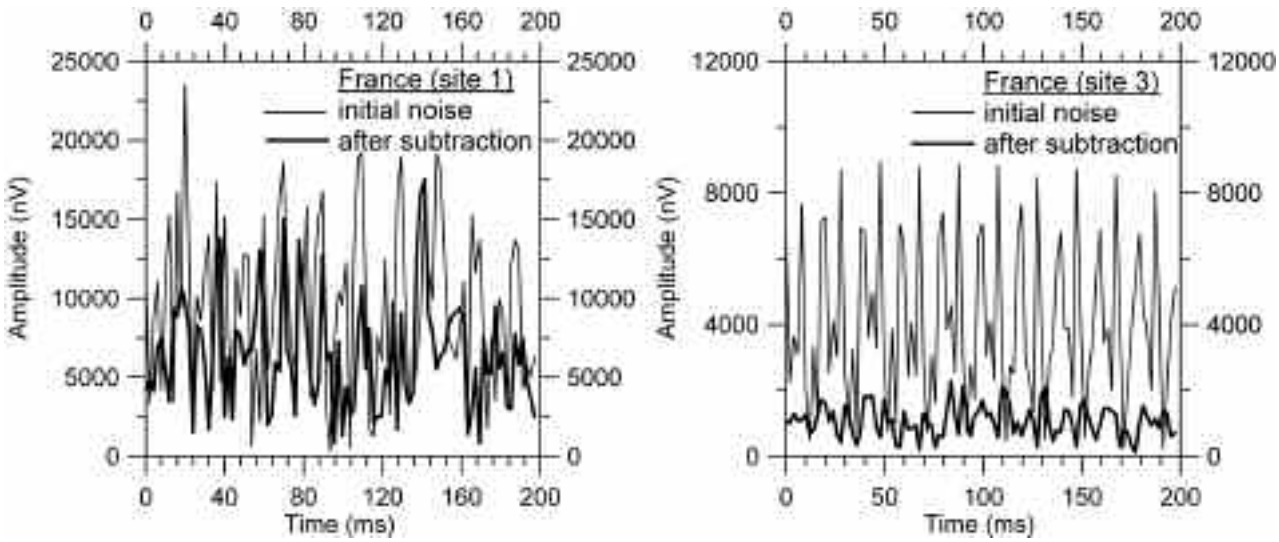

Fig. 8. Examples of the block subtraction application
Fig. 8. Ejemplos de aplicación del método de sustracción por bloques

the low-pass filter and do not influence MRS measurement accuracy. The few interfering harmonics (usually three, but sometimes five) are close to f_L. In the NUMIS system, synchronous detectors (3 or 5) are used for power-line harmonics estimation (amplitude, phase and frequency), in a manner very similar to that applied to signal processing. For each synchronous detector, the reference frequency is set equal to one of the few fundamental harmonics frequencies close to the Larmor frequency: f^k_{sd} =50k. The low-pass filter has a bandwidth of 5 Hz instead of 100 Hz. If the fundamental frequency is sufficiently stable, or varies slowly and thus can be considered stable during a few seconds period, the harmonics can be estimated using a noise record before the pulse (E_0=0 in Equations 1 and 2). Otherwise, a record after the pulse can be used, on the assumption that the noise is much larger than the signal ($p_k >> E_0$ for all $k \in K$, in Equations 1 and 2). Obviously, there is no need to compute the logarithm for the harmonics amplitude estimation (Equation 3).

Modeling results show that, using a one-second long record, the power-line harmonic frequency can be measured reliably to within an error of ±0.1 Hz. For example, assuming that for k^{th} harmonic

$$p_k >> (E_0 + \varepsilon(t))$$

and

$$\varphi_k = 0$$

phase

$$\Phi(t) = 2\Pi \cdot \delta f_k \cdot t$$

is calculated after the synchronous detector (Equation 4) by varying $\delta f_k=(f_{sd}-f_k)$ as shown in Figure 9. This example demonstrates that margins of error even smaller than 0.1 Hz error can easily be achieved but, in practice, non-regular noise may corrupt the phase measurements $\phi(t)$ and diminish the accuracy.

Filtering technique: notch filtering

When designing a low-pass filter for the MRS system, it should be kept in mind that the relaxation time of the magnetic resonance signal T^*_2 varies typically from 40 ms to 400 ms and this determines the band-

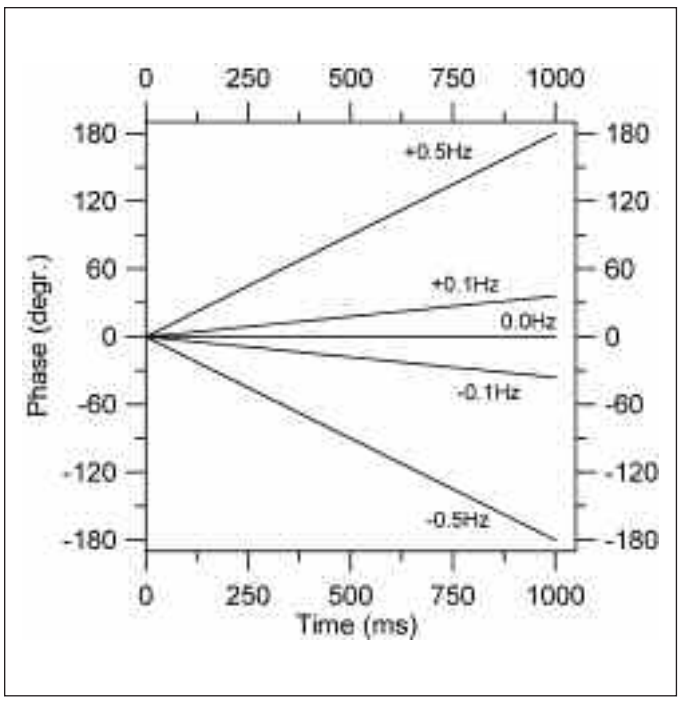

Fig. 9. Phase shift caused by different frequency offsets δf
Fig. 9. Desfase producido por diferentes desviaciones de la frecuencia δf

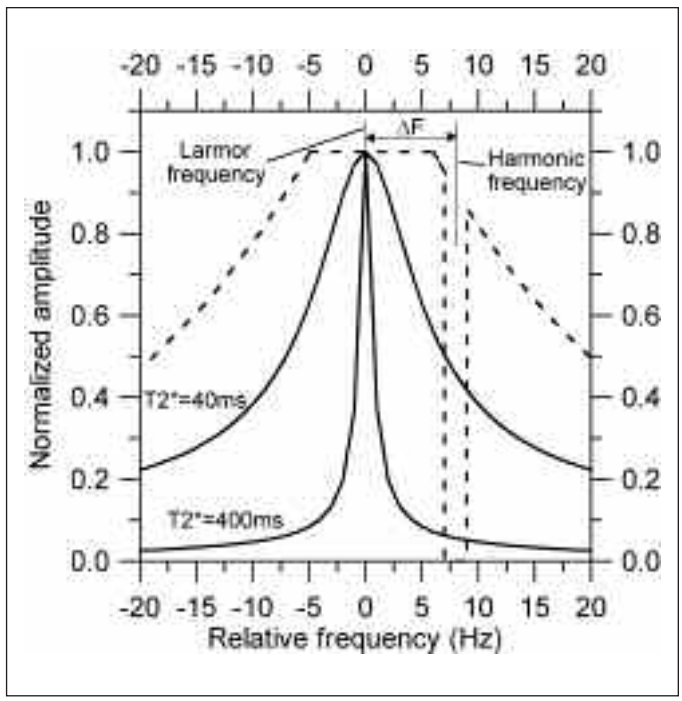

Fig. 10. Spectra of the exponential signal (solid lines) and combined low-pass and notch filter (dashed line)
Fig. 10. Espectro de la señal exponencial (línea continua) y combinación de filtros pasa-baja y notch (línea discontinua)

width of the filter. The Larmor frequency cannot be considered as constant, because it is affected by geomagnetic field variations within the volume investigated by MRS and also is unstable over time, and hence the bandwidth of the filter must be increased to about 4 Hz. The notch filter is centered on the power-line harmonic frequencies; as these are known only approximately, the filter cuts out ±1Hz bandwidth around each harmonic. A combined filter, consisting of a low-pass filter centered on the Larmor frequency and a ±1 Hz notch filter centered as close as possible to the Larmor frequency harmonic of the fundamental frequency, is depicted in Figure 10 (dashed line). It should be noted that the notch filter removes 3 or 5 harmonics, but they are not shown in Figure 10.

Whilst the sinusoid subtraction method subtracts the estimates of power-line harmonics without distorting or attenuating the signal of interest, the notch filter always cuts out a narrow frequency band and, therefore, the signal may be deformed. It is thus necessary to consider the distortion effect of such a notch filter on the magnetic resonance signal. Numerical modeling results show that application of the notch filter significantly improves accuracy of signal parameter estimation for all the power-line frequency offset values. The notch filter efficiently eliminates the sinusoidal noise and there is practically no distortion to the synthetic signal when $\Delta F > 4$ Hz. For smaller values of the frequency offset ($\Delta F \leq 4$ Hz), the notch filter corrupts the signal. However, the noise influence on unfiltered signals may be even more harmful and quite often leads to fitting instability. Consequently, the improvement in signal parameter estimation due to the filtering algorithm can be evaluated by considering the S/N for which the non-linear fitting algorithm becomes unstable as the critical value. The results are summarized in Table 1. Depending on the test site, the critical value of S/N varies between 0.8 and 0.1 without the notch filter and between 0.01 and 0.08 with the notch filter. The improvement in the critical S/N is between 2.3 and 10 times depending on the site.

Comparison of different filtering techniques

The efficiency of the filtering techniques was estimated using 40 consecutive noise records made at each

Test site	Critical S/N notch OFF	Critical S/N notch ON	Improvement in S/N
The Netherlands	0.16	0.07	2.28
France (site1)	0.8	0.08	10
France (site 2)	0.1	0.01	10

Table 1. Threshold of relible estimation of the MRS signal parameters
Tabla 1. Valores de los parámetros de estimación de fiabilidad de un SRM

of four test sites (France three, Netherlands one). Our results show that the efficiency of the noise filtering methods depends on the test site. The best results are obtained at Sites 2 and 3 (France) where the noise contains the largest percentage of 50 Hz harmonics (Figure 6). At the same site, notch filtering appears to be the most efficient for noise reduction as it cuts out the largest bandwidth. The sinusoid subtraction and the block subtraction are respectively less efficient. However, it should be remembered that when the Larmor frequency is close to one of the power-line harmonic frequencies, the notch filtering might also distort the signal of interest. So, depending on the noise and the frequency offset, a compromise must be made between removing the noise and keeping the signal undisturbed so that signal parameters can be estimated.

Basing on experience gained to date, the rule for filtering method selection is proposed (Table 2). It can be shortly summarized as following:

- When the frequency offset $|\Delta F|>8$ Hz, the notch filter is the most effective.
- When $|\Delta F|<8$ Hz, the notch filter may be too drastic and suppress important signal information for long relaxation times ($T^*_2>200$ ms) and, in this case, the subtraction techniques must be used.

Filter	T_2^*=100 ms	T_2^*=200 ms	T_2^*=400 ms
+/-1 Hz notch filter	ΔF>4 Hz	ΔF>6 Hz	ΔF>8 Hz
Sinusoid subtraction	ΔF<4 Hz	1<ΔF<6 Hz	2<ΔF<8 Hz
Block subtraction	ΔF<1 Hz	ΔF<1 Hz	ΔF<2 Hz

Table 2. Optimal selection of the filtering technique
Tabla 2. Optimización en la selección de la técnica de filtrado

Inversion of MRS measurements

Amplitude of MRS signal

For measuring MRS signal, a pulse of alternating current energizes the loop

$$i(t) = I_0 \cos(\omega_L t), \qquad 0 < t \le \tau \tag{10}$$

where I_0 and τ are respectively the pulse amplitude and duration and $\omega_L=\gamma B_0$ is the Larmor frequency. The pulse causes precession of the spin magnetization around the geomagnetic field, which produces a non-zero flip angle

$$\theta = \frac{\gamma B_{T\perp}(r)}{2I_0} q \tag{11}$$

where $q=I_0\tau$ is the pulse moment, $B_{T\perp}(r)$ is a perpendicular to the geomagnetic field component of the loop magnetic field, and $r=r(x,y,z)$ is the coordinate vector. The signal induced in the receiver loop is proportional to the sum of the flux of all precessing magnetic moments $M_\perp=M_0 \sin(\theta)$. With

$$M_0 = NB_0 \frac{\gamma^2 h^2}{4kT}$$

where N is the number of hydrogen protons per unit volume, T is the absolute temperature, h is the Planck constant and the Boltzmann constant $k=1.3805.10^{-23}$ [J/°]. Since $N=6.692.10^{28}$ [/m³], it is found that $M_0=3.287.10^{-3}B_0$ at 293°K (20°C). Neglecting the higher harmonics of the pulse and a possible frequency offset between the Larmor frequency and the current frequency, the induction in the coincident Tx/Rx loop voltage thus becomes (Legchenko and Valla, 2002)

$$E_0(q) = \frac{M_0\omega_L}{I_0} \int_V B_{T\perp}(r) e^{j2\varphi_0(r)} \sin(\theta(r,q)) w(r) dV(r) \tag{12}$$

where φ_0 is the phase shift caused by electrically conductive rocks, and $0 \le w(r) \le 1$ is the water content. As both the magnetic moment per unit volume M_0 and the Larmor frequency ω_L are proportional to the geomagnetic field, it follows from Equation 12 that the

amplitude of the magnetic resonance signal depends on the geographical location of the investigated area $E_0 \sim B^2_0$ (Legchenko *et al.,* 1997). Assuming that the stratification is horizontal, and the vertical distribution of resistivity is known, Equation 12 of the signal amplitude E_0 can be simplified to a Fredholm linear integral equation of the first kind (Legchenko and Shushakov, 1998)

$$E_0(q) = \int_0^L K(q,z)w(z)dz \qquad [13]$$

where

$$K(q,z) = \frac{M_0\omega_L}{I_0} \int_{x,y} B_{T\perp}(r)\sin(\theta(r,q))dxdy$$

Numerical results show that distant protons produce a negligibly small signal and, hence, integration can be limited by approximately $L=(x^2+y^2)^{1/2}<3\sqrt{S}$, where S is the loop surface. However, practically $L=1.5\sqrt{S}$ can be considered as the maximum reliable depth of water detection by MRS, and a cube with side $1.5\sqrt{S}$ as the approximate investigating volume. It should be noted that in heterogeneous geological environments, MRS data about aquifers are the averages of readings for a volume proportional to the size of the loop.

Regularization of MRS inversion

Different inversion schemes can be found in the literature (Guillen and Legchenko, 2002a; 2002b; Hertrich and Yaramanci, 2002; Legchenko and Shushakov, 1998; Mohnke and Yaramanci, 2002). Some of them are also presented in Yaramanci and Hertrich (2007, this Issue). However, resolution of MRS inversion is mostly defined by the MRS integral equation and selection of the inversion scheme does not change the general nature of presented in this paper results.

Tikhonov regularization method

The vertical distribution of water content w(z) is resolved by Equation 13. This linear equation may be solved by projecting it onto finite dimensional subspace, and approximated by the projected equation

$$\sum_j \varphi_j(q_i)w_j = E_{0i} \qquad [14]$$

where i=1,2,….I j=1,2,…..J and $\varphi_j(q)$ is a set of kernel vectors obtained by projecting the kernel K(q,z) on a set of basis functions $b_j(z)$, so that

$$w(z) = \sum_j w_j b_j(z) \qquad [15]$$

and

$$\varphi_j(q) = \int_0^L K(q,z)b_j(z)dz \qquad [16]$$

From a physical point of view, the problem allows the basis functions to be assumed as box-car functions. Hence, the kernel vectors are the elementary responses from the layers of water (w_j=1), characterized by their depth z and thickness Δz. When the depth intervals are

$$0 \le z \le L, \quad \Delta z_j = z_{j+1} - z_j, \quad L = \sum_{j=1}^{J} \Delta z_j \qquad [17]$$

the basis functions are

$$b_j(z_j \le z < z_{j+1}) = 1, \quad b_j(z < z_j, z \ge z_{j+1}) = 0 \qquad [18]$$

and the kernel vectors are

$$\varphi_j(q) = \int_{z_j}^{z_{j+1}} K(q,z)dz \qquad [19]$$

In a matrix notation, projected Equation 14 can be written as

$$\mathbf{Aw} = \mathbf{E}_0 \qquad [20]$$

where $\mathbf{A}=[a_{i,j}]$ is a rectangular matrix of I x J with the elements $a_{i,j}=\varphi_j(q_i)$, $\mathbf{E_0}=(E_{01},E_{02},\ldots,E_{0i},\ldots E_{0I})^T$, $E_{0i}=E_0(q_i)$ being the set of experimental data, $\mathbf{w}=(w_1,w_2,\ldots, w_j,\ldots w_J)^T$, $w_j=w(\Delta z_j)$ being the vertical distribution of water content, and the symbol T denoting transposition.

Numerical solution of matrix Equation 20 is highly dependent on the choice of basis functions. For a unique and stable solution, the kernel vectors must be linearly independent. In this case, the number of

the basis functions is small and, in spite of the uniqueness, such a solution has no practical importance due to a large discretization error. Increasing the number of basis functions reduces the error due to discretization, but the stability of the solution suffers due to ill-conditioning of the problem.

Stability of the matrix $\mathbf{C}=\mathbf{A}^T\mathbf{A}$ can be estimated using the concept of condition number

$$\mathrm{cond}(\mathbf{C}) = (\lambda_{max} / \lambda_{min}) \geq 1 \qquad [21]$$

where λ_{max} , λ_{min} are the maximum and minimum eigenvalues of the matrix **C**. In general, a linear system with a small condition-number value is more stable than a system with a large one. For L_2 norm, $\mathrm{cond}(\mathbf{A})=\sqrt{\mathrm{cond}(\mathbf{C})}$; hence, the linear dependence between the kernel vectors affects not only the stability of the matrix **C** but also the stability of the matrix **A**.

The condition number of the matrix **A** can be used for estimating the relative error amplification

$$\sqrt{\left(\left|\delta w(z)\right|^2 / \left|w(z)\right|^2\right)} \leq \mathrm{cond}(\mathbf{A})\sqrt{\left(\left|\varepsilon(q)\right|^2 / \left|E_0(q)\right|^2\right)} \qquad [22]$$

where $|\varepsilon(q)|^2$ is the experimental data error (noise), $|E_0(q)|^2$ is the signal, $|\delta w(z)|^2$ is the error of the solution, and $|w(z)|^2$ is the solution itself. The condition number is the less optimistic evaluation of the error amplification.

In NUMIS system, the inversion was carried out according to the well-known Tikhonov regularization method (Tikhonov and Arsenin, 1977). In order to find an approximate solution of the Equation 20, this method supposes minimization of the Tikhonov functional

$$M_\alpha(\mathbf{w}) = \left\|\mathbf{A}\mathbf{w}_\alpha - \mathbf{E}_{0\varepsilon}\right\|_{L2} + \alpha\left\|\mathbf{w}_\alpha\right\|_{L2} = \min \qquad [23]$$

where the matrix **A** is a product of discretization of the Equation 12, $\mathbf{E}_{0\varepsilon}$ is the vector of the experimental data contaminated by the noise $\varepsilon=||\varepsilon||_{L2}$, $\mathbf{w}_\alpha$ is the solution vector that minimizes Equation 23, and $\alpha>0$ is the parameter of regularization.

To solve this minimization problem, we followed the discrepancy principle introduced by Morozov (1966), which is based on the fact that for erroneous data, it does not make much sense to have the residual $||\mathbf{A}\mathbf{w}_\alpha - \mathbf{E}_{0\varepsilon}||_{L2}$ smaller than the experimental error. Hence, for a given $\varepsilon>0$, we need to find a solution with a residual $||\mathbf{A}\mathbf{w}_\alpha - \mathbf{E}_{0\varepsilon}||_{L2} \leq \varepsilon$ and stabilize it by making $||\mathbf{w}_\alpha||_{L2}$ small. $\mathbf{w}_\alpha$ is an approximation of the solution of Equation 20. When $\varepsilon\to0$, $\alpha(\varepsilon)\to0$ and $\mathbf{w}_\alpha\to\mathbf{w}$. For the optimization itself we used the conjugate gradient method (Stoer and Bulirsch, 1980).

Application of the regularization (not necessary the same as presented above scheme) allows damping oscillations of the solution caused by the noise. But it is also smoothing the solution thus diminishing the resolution of the method.

Discretization of the integral equation

The condition number of the matrix **A** can be used for estimating the relative error amplification (Equation 22). It depends on discretization of Equation 12. If we assume that $\Delta z_1 < \ldots < \Delta z_j < \ldots < \Delta z_J$ and make Δz_j increasing with depth respecting the exponential low then the number of layers (J) will allow us to manage the sensibility of inversion to the experimental noise. Numerical calculations of the condition number of the matrix **A** versus the layers number (Figure 11) confirm the existence of relationship between the two parameters. The eigenvalues were calculated by the standard Jacobi method (Stoer and Bulirsch, 1980) for $\mathbf{C}=\mathbf{A}^T\mathbf{A}$ matrix and afterwards, as $\mathrm{cond}(\mathbf{A})=\sqrt{\mathrm{cond}(\mathbf{A}^T\mathbf{A})}$ for **A** itself. For this example, calculations were performed using a circular antenna of 100 m diameter, a vertical geomagnetic field with the magnitude of 58685.45 nT, and the corresponding Larmor frequency of protons in water $\omega_L/2\pi=2500$ Hz.

Thus, when the noise is small number of layers in the matrix **A** may be increased thus improving the vertical resolution of the inversion results. But when experimental data are corrupted by noise, increase of the number of layers cannot improve the resolution limited by the signal to noise ratio.

Selection of the parameter of regularization

In NUMIS system, the noise magnitude is measured before the pulse (Figure 1). After stacking and filtering it can be estimated using Equation 6. Equation 23 is than resolved following the discrepancy principle $||\mathbf{A}\mathbf{w}_\alpha - \mathbf{E}_{0\varepsilon}||_{L2} \leq \varepsilon$, with ε estimated from the noise records and varying the parameter of regularization α at each step of optimization. When the minimum is found, $\mathbf{w}_\alpha$ is an approximation of the solution we are looking for. NUMIS inversion software allows also setting the parameter of regularization manually thus permitting to users to adjust solution semi-manually.

Thus, the parameter of regularization is a tool that allows finding a compromise between the accuracy of

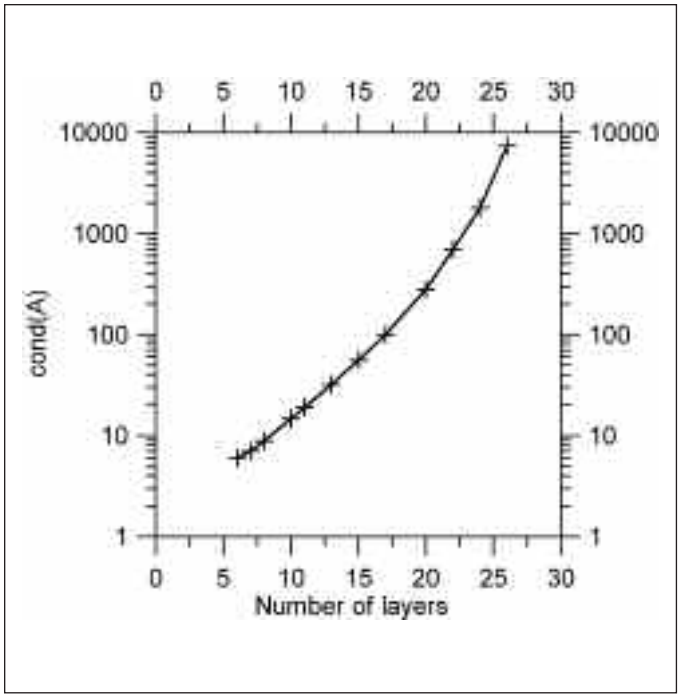

Fig. 11. Condition number of matrix **A** versus the number of layers computed for a 100-m-diameter loop
*Fig. 11. Valor de condición de la matriz **A** en función del número de capas utilizadas en el cálculo, para una antena de 100 m de diámetro*

fitting of the experimental data and smoothness of the solution. Obviously, if data are erroneous then more weight is given to smoothness condition. If data are accurate then the regularization scheme allows to the solution to be less smooth thus improving the resolution. When the parameter of regularization is underestimated, it does not improve the resolution because of the solution will be contaminated by noise. If the parameter of regularization is overestimated then some information contained in experimental data will be lost.

Depth of investigation with MRS method

The magnetic resonance signal is sensitive to different natural factors what makes the performance of the method site-dependent. The most common and practically important variations in the magnetic resonance signal are related to the electrical conductivity of rocks and the natural geomagnetic field (Semenov, *et al*., 1989; Shushakov, 1996; Legchenko, *et al*., 1997; Valla and Legchenko, 2002).

The electrically conductive subsurface attenuates alternative electromagnetic fields by a factor characterized by the "skin depth" that is proportional to $\sqrt{\rho/f}$, where ρ is the resistivity of the subsurface, and f is the frequency of the electromagnetic field. The electrical conductivity is a major factor that is limiting the depth of investigation with MRS. Indeed, from Equation 12 follows that if the loop size is increased, the depth of investigation should be also increased. However, at the Larmor frequency around 2000 Hz even in rocks considered as "non-conductive" (for example, 100 ohm-m half space) the skin depth is about $z_s=503\sqrt{\rho/f} \approx 112$ m. Consequently, when using a typical MRS setup (square loop of 75x75 m or 100x100 m, or circular loop with D=100 m), the average depth of investigation (about 100 m) is smaller than the skin depth and the electrical conductivity has relatively minor effect on the MRS signal. If we try to increase the loop thus looking for larger depth of investigation then the depth we are looking for will be greater than the skin depth and the conductivity will have major effect on the MRS signal.

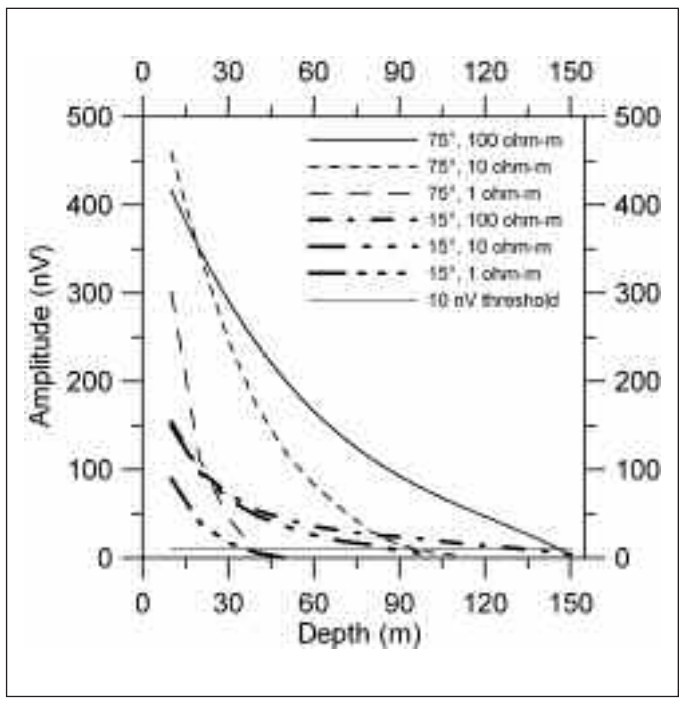

Fig. 12. Amplitude of MRS signal versus the depth a 1-m-thick layer of free water (w=100%) calculated for different geomagnetic fields (15°, 30000 nT; and 75°, 60000 nT) and half-space resistivity (100, 10 and 1 ohm-m)
Fig. 12. Amplitud de la señal SRM de una capa de 1 m de potencia saturada de agua (w=100 %) en función de la profundidad, calculada para diferentes campos geomagnéticos (15°, 30000 nT; y 75°, 60000 nT) y resistividades del medio (100, 10 y 1 ohm-m)

The Larmor frequency used in MRS is proportional to the geomagnetic field magnitude ($f_L \sim B_0$). Consequently, in areas with a low geomagnetic field (towards the equator), the frequency is smaller, and the attenuation caused by the subsurface is less important than in areas with a high geomagnetic field (towards the poles). However, the magnetic resonance response is proportional to square of the geomagnetic field ($E_0 \sim B^2_0$), what improves the signal to noise ratio in areas with a high geomagnetic field even taking into account the attenuation caused by the subsurface.

A numerical demonstration of influence of these natural factors on the maximum depth of investigation of the MRS method is presented in Figure 12. Amplitude of a one meter thick infinite horizontal layer of water with 100% of the water content is depicted versus the depth of the layer. Calculations were performed for different geomagnetic fields and half-space resistivity using standard configuration: a square loop with a side of 100 m and a maximum pulse of 15000 A-ms. In noiseless environment a signal detection threshold for NUMIS^{PLUS} system is about 10 nV.

We can see that detection of small signals and hence the depth of investigation with MRS is directly proportional to the noise magnitude. Obviously, in presence of noise smaller signals cannot be reliably measured and consequently the depth of investigation will be diminished. For example, in noiseless environment (10 nV threshold) the depth of water detection in 10 ohm-m half-space and considering 75° geomagnetic field will be about 95 m. With the noise magnitude of 50 nV, it will be diminished to 75 m approximately. It should be also reminded that MRS signal is proportional to water volume in the subsurface and hence, aquifers containing larger amount of water can be detected at larger depth.

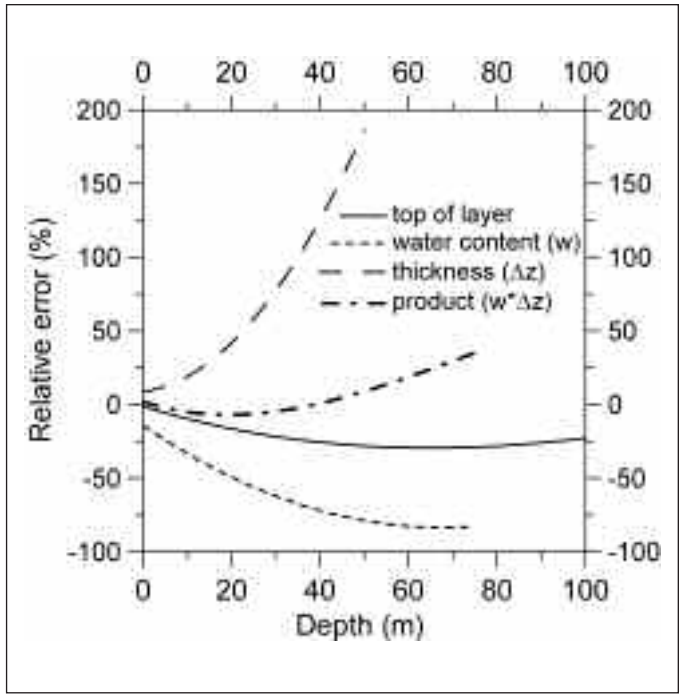

Fig. 13. Numerical modeling: resolution of a 10 m-thick layer when using 100 m-side square loop
Fig. 13. Modelado numérico: resolución de una capa de 10 m de potencia, utilizando una antena cuadrada de 100 m de lado

Resolution of MRS method

The vertical resolution of the MRS method depends on the magnetic field created by the loop; the larger the gradient of the field, the better the resolution. The magnetic field of the circular or square loop is well known; the gradient of the field is large close to the surface and decreases with increasing depth. Consequently, the resolution of the NMR is also better close to the surface. The vertical resolution corresponds to thicknesses of the basis functions, and hence,

$$\Delta z_1 \le \Delta z_2 \le ... \le \Delta z_j \le .. \le \Delta z_J \qquad [24]$$

In MRS it is impossible, for a particular layer, to know both the layer thickness and the water content, what is giving rise to layer equivalence. Two layers at the depth z_e with the thicknesses $\Delta z_1, \Delta z_2 < \Delta z_e$ are equivalent if $w_1 \Delta z_1 = w_2 \Delta z_2$. The equivalent layers cannot be resolved. The thickness Δz_e is defined by the vertical resolution of the method which depends on the magnetic field created by the loop; the larger the gradient of the field, the better the resolution. Figure 13 shows the relative errors of resolution for a synthetic model consisting of a 10-m-thick layer (w=20%) versus the layer depth. A square 100-m-side loop is assumed. The errors were calculated as

$$\varepsilon = 100\% x (P_{inv} - P_{mod}) / P_{mod}$$

where P_{inv} and P_{mod} are, respectively, a parameter from the inversion and its true value given by the model. It can be seen that both the water content and the thickness are better resolved when the layer is close to the loop, and that errors increase with distance from the loop. At a depth greater than about one half of the loop side, the 10-m-thick layer cannot be resolved.

However, note that the resolution accuracy of the product w x Δz is much better.

To numerically demonstrate influence of the noise on the inversion accuracy, we used a two-layer model consisting of two 10-m-thick horizontal, homogeneous, infinite water-saturated layers situated in 100 ohm-m half-space at depths of 10 and 30 m respectively. The water content of each layer was taken to be equal to 0.2 (w=0.2), corresponding to 20% of free water, and the geomagnetic field was assumed to be equal to 60000 nT with the inclination of 75°. A 100 m diameter circular antenna was used for calculating the MRS signal. Experimental errors were simulated by adding zero mean random noise to the model data. The inversion results are presented in Figure 14. Inversion (solid line) fits the model quite well (dashed line) when S/N=1000 (Figure 14a). However, even without noise resolution of the model is not perfect because it is limited by the non-uniqueness of the inverse problem. It is a fundamental limitation of the accuracy of MRS results. When S/N=5 (Figure 14b), two layers are not resolved. Inversion shows just one layer located incorrectly. When S/N=1 (Figure 14c), the fit to the model is very poor. In all three cases inversion is stable and a good mean square fit is obtained for both the theoretical curves and the model data (right hand graphs). However, when noise is getting larger resolution of the inversion is diminishing and it acts as a low pass filter.

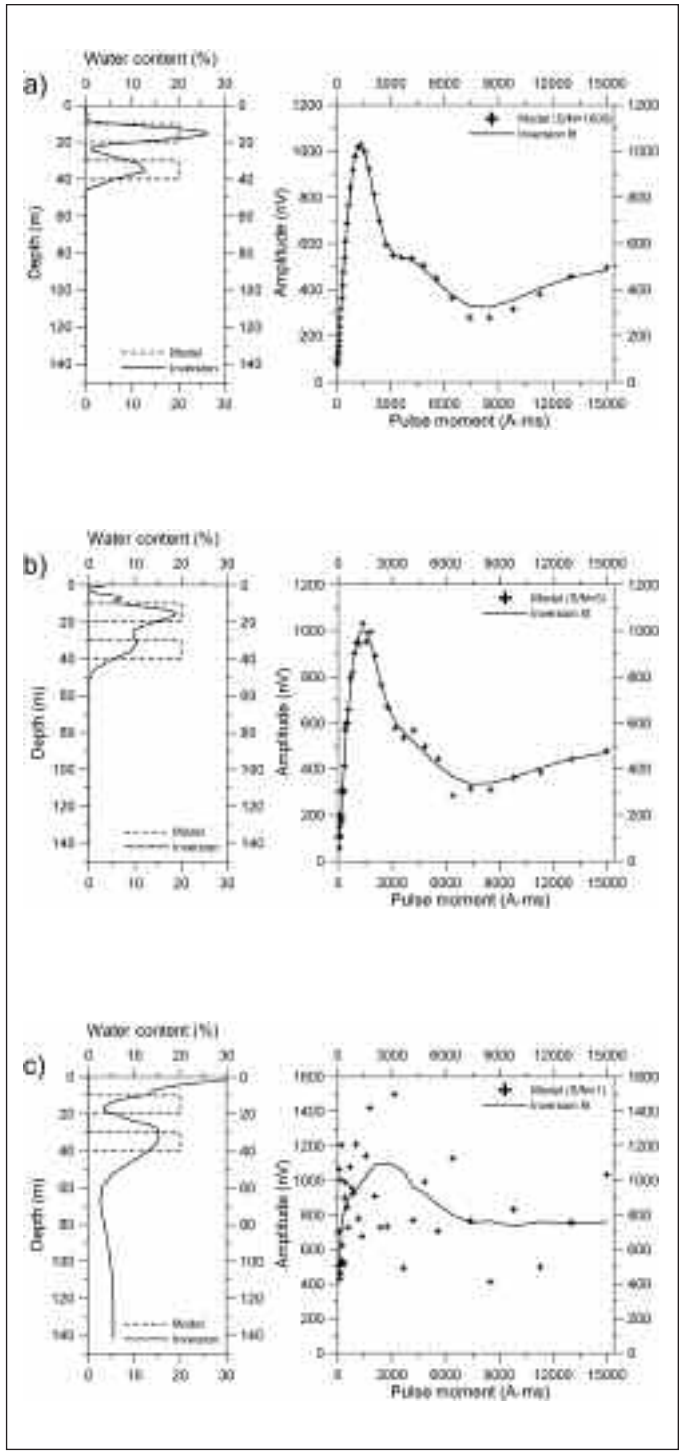

Fig. 14. Numerical modeling: example of resolution of two 10 m-thick layer with different signal to noise ratios: a) S/N=1000; b) S/N=5; c) S/N=1. Left hand graph – the vertical distribution of the water content; right hand graph – synthetic signal and inversion fit
Fig. 14. Modelo numérico: ejemplo de resolución para un modelo de dos capas de 10 m de potencia, con diferentes relaciones de señal y ruido S/N. a) S/N=1000; b) S/N=5; c) S/N=1. En los gráficos de la izquierda se representa la distribución vertical del contenido de agua; en los de la derecha, la señal del modelo y el ajuste de inversión

Estimation of MRS data quality

Currently, the MRS method is able to detect water in aquifers composed of non-magnetic rocks. The magnetic resonance signal may vary from 0 to about 4500 nV. Typical range for Europe is 0 – 500 nV, but for igneous rocks it is 0 – 150 nV. NUMIS^{PLUS} instrument has an instrumental noise which can be decreased by a stacking process down to about 3-5 nV. That puts the threshold of reliable measurements of magnetic resonance signal to 10 nV approximately.

For MRS data quality estimation, the following parameters can be used:

1) External noise level after stacking and filtering is compared with the NUMIS instrumental noise as EN/IN=(ext. noise)/(instr. noise)= noise/5. When the magnetic resonance signal is very small, the stacking should be carried out until EN/IN≈1. If EN/IN≈1 then the sounding can be considered to be of a good quality, even if the signal has not been detected.
2) The signal to noise ratio S/N=signal/noise. Usually data are considered of acceptable qual-

ity when S/N>2. In this case, a *quantitative* interpretation of MRS data is possible through inversion procedure, and reliable information about aquifers can be derived from MRS data. When S/N>2, it is not necessary to have EN/IN≈ 1. If EN/IN≈1 and S/N=1 (signal is not detected) then the quantitative interpretation of MRS data is not possible. In this case MRS reveals that volume of free water in the subsurface is smaller than the threshold of the instrument.

3) When EN/IN>1 and S/N ≈ 1 the sounding cannot be considered as of a good quality. In this case, the only conclusion can be derived from the data is that the amplitude of MRS signal is smaller than the noise level. For example, if EN/IN=5 and S/N=1 then one can conclude that if there is a signal it is smaller than 25 nV (considering IN=5 nV). However, inversion of MRS measurements with S/N ≈ 1 allows a *qualitative* interpretation. The qualitative interpretation reveals only an estimation of maximum possible free water volume inside of the loop area. This estimation only guarantees that it is not possible to have more water than is given by this estimation. The qualitative interpretation does not guarantee that there is water in the subsurface.

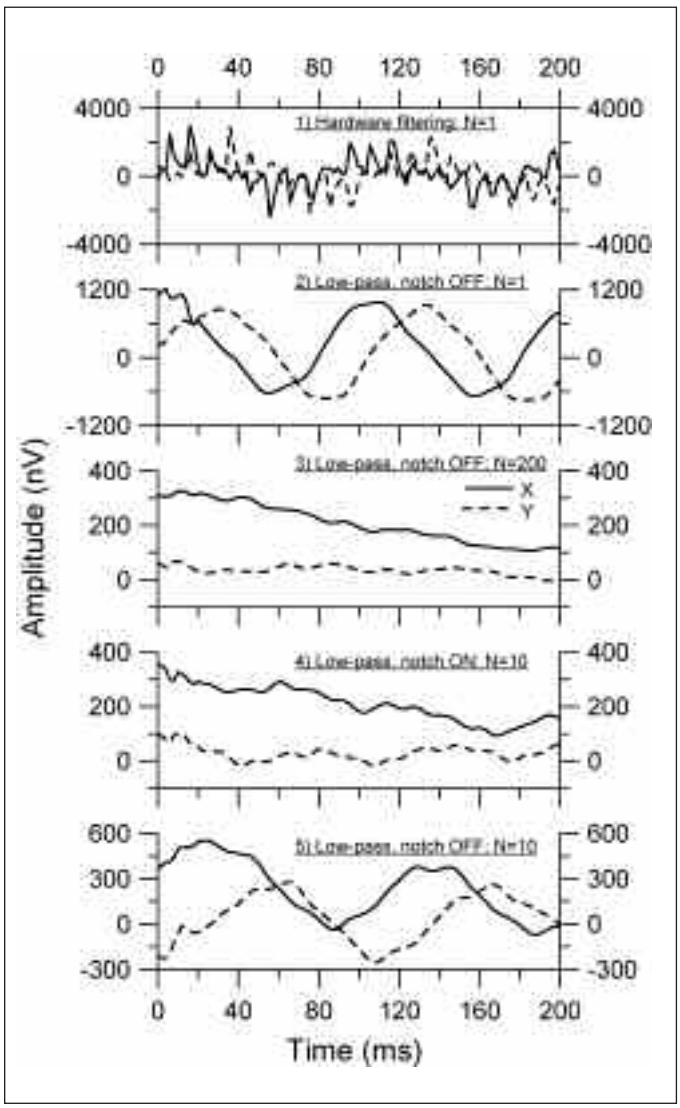

Fig. 15. Field example: filtering of signal records
Fig. 15. Ejemplos de mediciones reales mostrando el efecto de diversos métodos de filtrado en el registro

Example of Processing of real data

The results obtained in France with NUMIS instrumentation using a 75-m-side square loop can be used to demonstrate the method. Noise magnitude was found to be about 900 nV (corresponding EM field of $16x10^{-11}$ T approximately) and, for this level of a noise, a stacking procedure was necessary to improve the signal to noise ratio. Spectral analysis revealed a high percentage of 50 Hz harmonics, which suggested that one of the power-line filtering techniques may be suitable. The Larmor frequency, measured with a proton magnetometer, was 2010 Hz. As $|\Delta F|>8$ Hz, the ± 1 Hz notch filtering scheme could be applied and records were filtered before stacking. Two soundings were performed at the same site: a) with 200 stacks without notch filtering; b) with 10 stacks that were processed with and without notch filtering. It was considered that sounding (a) provided true data and it was therefore compared with two other soundings.

Figure 15 shows NUMIS records (after the synchronous detector) made with the same value of the pulse moment containing both the signal and the noise: 1) one stack after only hardware-filtering; 2) same as (1), but with the low-pass filter without notch filtering; 3) after 200 stacks and the low-pass filter, without notch filtering; 4) after 10 stacks and the low-pass filter, with notch filtering; 5) same as (4) without notch filtering. It can be seen that application of notch filtering allows signal recovery using 10 stacks with about the same degree of accuracy as using 200 stacks without notch filtering.

Signal parameters estimated for these three soundings against the pulse moment are shown in Figure 16. One can see that the results obtained using 10 stacks and applying the notch filtering are close to those made with 200 stacks. As the signal frequency estimate corresponds well to the proton magnetome-

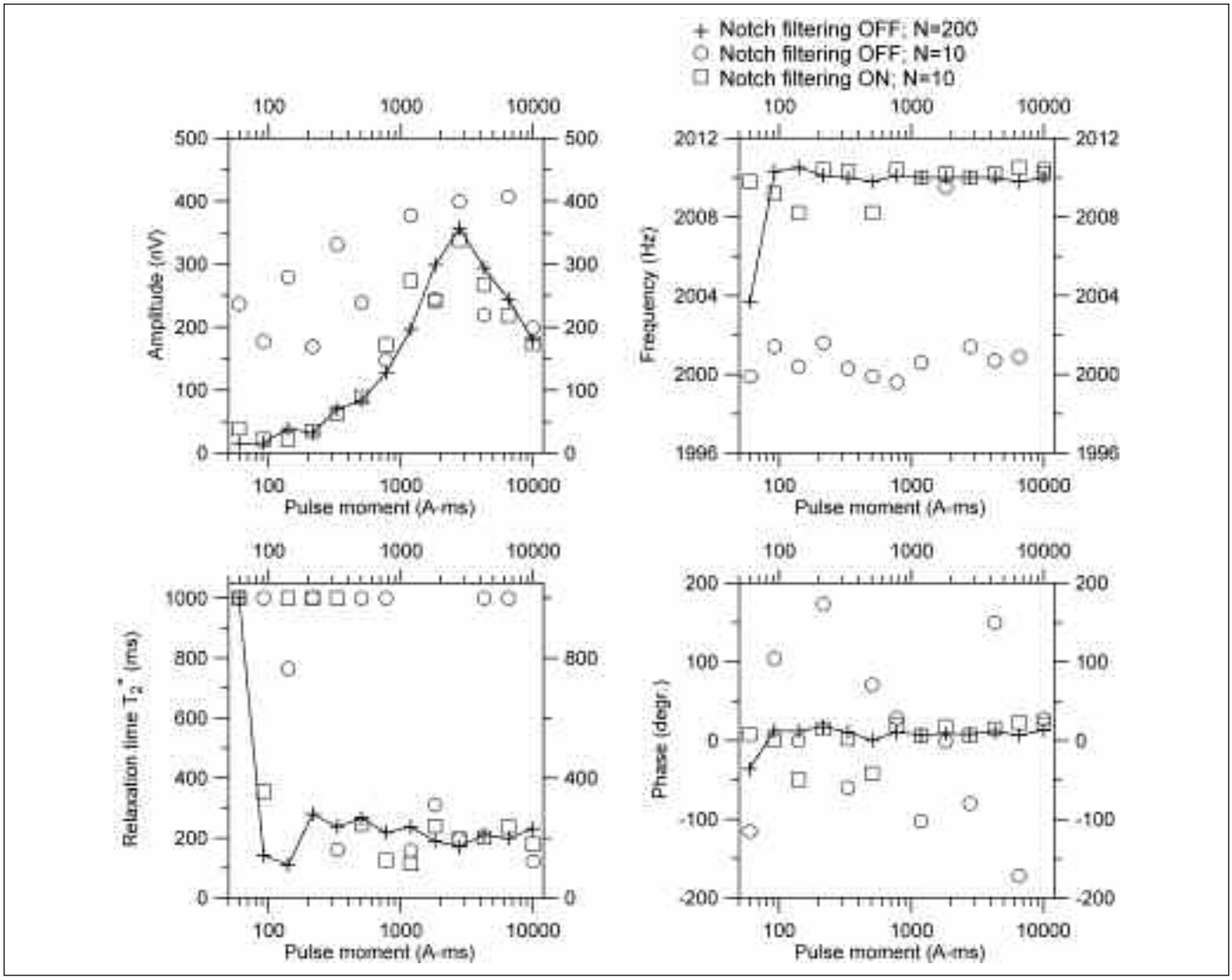

Fig. 16. Field example: MRS signal estimates when using the different filtering procedures
Fig. 16. Ejemplos de mediciones reales: señales de SRM obtenidas con diversos métodos de filtrado

ter measurements (2010 Hz) and the phase varies smoothly, it can be concluded that the magnetic resonance signal was detected reliably. Using 10 stacks without the notch filtering, the signal frequency estimate is about 2000 Hz which corresponds to the 40th harmonic of 50 Hz. Unlike the magnetic resonance signal frequency, the power-line frequency is not synchronized with the pulse and, thus, the phase derived from the records is understandably non-regular.

Inversion of these data was performed using standard NUMIS inversion routine. Estimation of the data quality (Table 3) reveals that two soundings (Notch=ON, N=10; and Notch=OFF, N=200) have similar quality and inversion provide reliable results. For one sounding (Notch=OFF, N=10) measurements have poor signal to noise ratio and the only information that can be derived from these data is that we cannot have more than 30% of the water content. Note, that the fitting error is only twice greater in comparison with two other soundings. In spite of this, we cannot trust to inversion results because of S/N is poor. Comparison of MRS results with the corresponding borehole log (Figure 17) shows that the aquifer was well detected in two cases; using the data acquired with 200 stacks, and with 10 stacks and notch filtering. Comparison between these two data sets (water content w(z) and relaxation time $T^*_2(z)$) also shows reasonable agreement. Inversion of the

Sounding	S/N	EN/IN	Fitting error	Quality
Notch OFF, N=10	1.1	41	25.2%	Qualitative interpretation
Notch ON, N=10	2.9	7.7	12.2%	Quantitative interpretation
Notch OFF, N=200	2.7	8.2	11.9%	Quantitative interpretation

Table 3. Example of processing of real data: quality estimation
Tabla 3. Ejemplo de proceso de datos reales: estimación de la calidad

data set with 10 stacks without notch filtering provides unrealistic results that can be easily explained as lack of accuracy due to power-line noise.

Presented examples show that we can obtain similar results applying or not the notch filtering. However, let us estimate duration of the data acquisition. One sounding consists of the signal parameter estimation for 10 to 20 different values of the pulse parameter. Each value of the pulse parameter had stacking applied. For the NUMIS system, the time interval between two consecutive records is about six seconds. Thus, the time spent in the field could be estimated as 10 x 10 x 6 = 600 s (plus time for the loop setup) when 10 stacks are used. This can be compared with the 200 x 10 x 6 = 12000 s necessary for 200 stack soundings.

Conclusions

Both the depth of investigation and resolution of the MRS method depend on signal to noise ratio. If measured data are corrupted by noise, it will have an effect on the accuracy and reliability of MRS results. Consequently, if in the field the MRS signal cannot be measured with an acceptable signal to noise ratio then the only conclusion derived from these data would be that MRS cannot be applied in this site.

For improving the signal to noise ratio different filtering techniques could be applied. Selection of the filtering scheme depends on the noise origin. In any case, application of the stacking is necessary. A large number of repetitive measurements is often required for stacking and consequently one sounding may take from one to twelve hours.

Acknowledgements

Development of the MRS method was carried out since 1979. It was starting in Russia under the guid-

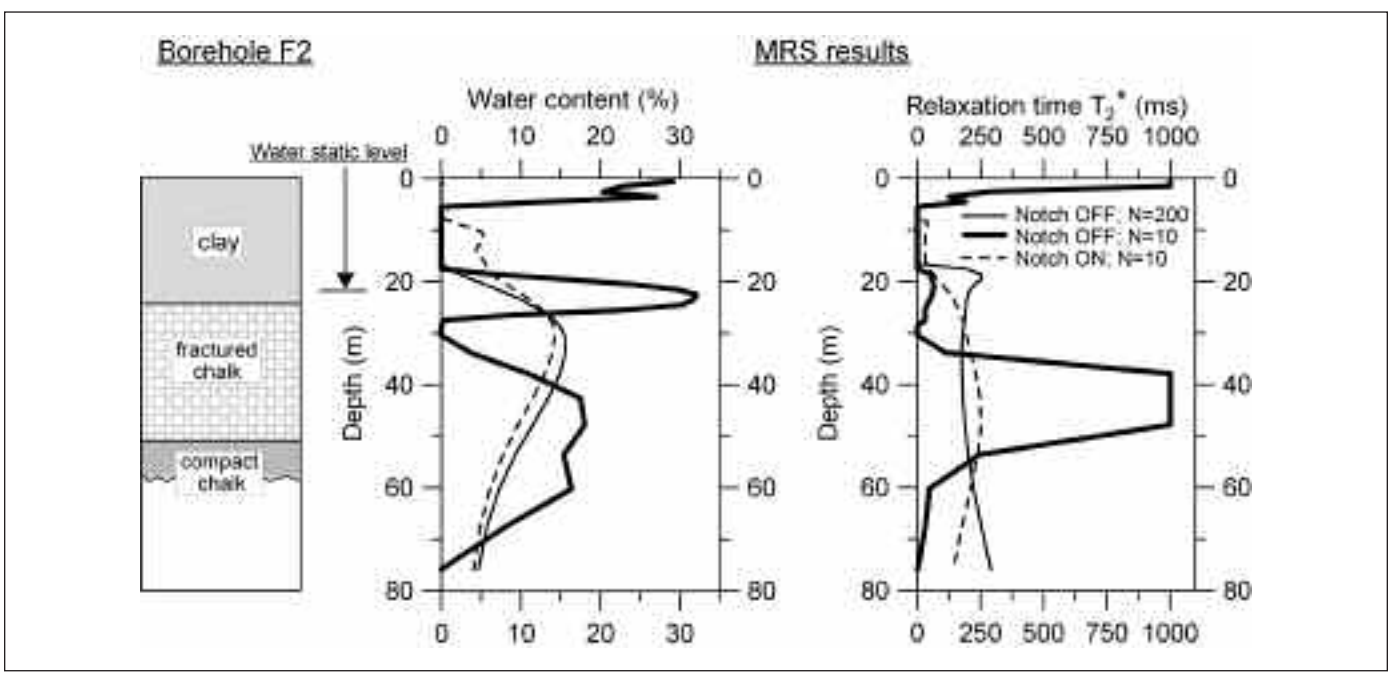

Fig. 17. Field example: borehole log and MRS inversion results when using the different filtering procedures
Fig. 17. Ejemplos de mediciones reales: comparación de la columna litológica con los resultados de la inversión de los datos de SRM según los diversos sistemas de filtro utilizados en su registro

ance of A.G. Semenov, the inventor of the MRS method. In this paper summary of the research activity carried out for years in collaboration with number of colleagues in different countries is presented. Author is particularly thankful to P. Valla, J-M. Baltassat, J. Bernard, M. Boucher, A. Beauce, J-F. Girard, M. Descloitres, J. Pierrat, J-M. Vouillamoz (France); M. Schirov and O. Shushakov (Russia); U. Yaramanci, M. Hertrich and M. Braun (Germany); J. Roy and M. Lubchinski (the Netherlands), A. Mazzella, P. Haeni, E. White and J. Lane (USA); J. Plata and F. Rubio (Spain); and other colleagues.

References

Bernard, J. 2007. Instruments and field work to measure a Magnetic Resonance Sounding. *Boletín Geológico y Minero,* 118(3), 459-472.

Butler, K.E. 2001. Comment on "Design of a hum filter for suppressing power-line noise in seismic data. *Journal of Environmental and Engineering Geophysics*, 6 (2), 103-104.

Butler, K.E. and Russell, R.D. 1993. Subtraction of powerline harmonics from geophysical records. *Geophysics*, 58, 898-903.

Guillen, A. and Legchenko, A. 2002a. Application of linear programming techniques to the inversion of proton magnetic resonance measurements for water prospecting from the surface. *Journal of Applied Geophysics*, 50, 149-162.

Guillen, A. and Legchenko, A. 2002b. Inversion of Surface Nuclear Magnetic Resonance data by an adapted Monte-Carlo method applied to water resource characterization. *Journal of Applied Geophysics* 50, 193-205.

Hertrich, M. and Yaramanci, U. 2002. Joint inversion of Surface Nuclear Magnetic Resonance and Vertical Electrical Soundings. *Journal of Applied Geophysics* 50, 179-191.

Legchenko, A.V., Beauce, A., Guillen, A., Valla, P. and Bernard J. 1997. Natural variations in the magnetic resonance signal used in PMR groundwater prospecting from the surface. *European Journal of Environmental and Engineering Geophysics*, 2, 173-190.

Legchenko, A.V., and Shushakov, O.A. 1998. Inversion of surface NMR data. *Geophysics* 63 (1), 75-84.

Legchenko, A. and Valla, P. 1998. Processing of surface proton magnetic resonance signals using non-linear fitting. *Journal of Applied Geophysics* 39, 77-83.

Legchenko, A. and Valla, P. 2002. A review of the basic principles for proton magnetic resonance sounding measurements. *Journal of Applied Geophysics* 50, 3-19.

Legchenko, A. and Valla, P. 2003. Removal of power line harmonics from proton magnetic resonance measurements. *Journal of Applied Geophysics* 53, 103-120.

Marquardt, D. 1963. An algorithm for least-squares estimation of non-linear parameters. *Journal of the Society for Industrial and Applied Mathematics* 11, 431-441.

Max, J., 1981. *Méthodes et techniques de traitement du signal et applications aux measures physiques*, tome II, troisième édition, Masson, Paris, 238 pp.

Mohnke, O. and Yaramanci, U. 2002. Smooth and block inversion of surface NMR amplitudes and decay times using simulated annealing. *Journal of Applied Geophysics* 50, 163-177.

Morozov, V.A. 1966. On the solution of functional equations by the method of regularization. *Soviet Mathematics Doklady* 7, 414-417 (English translation).

Plata, J.L. and Rubio, F.M. 2007. Basic theory of the Magnetic Resonance Sounding Method. *Boletín Geológico y Minero,* 118(3), 441-458.

Shushakov, O.A. 1996. Groundwater NMR in conductive water. *Geophysics* 61, 998-1006.

Semenov, A.G., Schirov, M.D., Legchenko, A.V., Burshtein, A.I. and Pusep, A.Y. 1989. *Device for measuring the parameter of underground mineral deposit*. Great Britain Patent 2198540B.

Stoer, J., Bulirsch, R. 1980. *Introduction to numerical analysis*. Springer-Verlag Berlin. 609 pp.

Tikhonov, A. and Arsenin ,V. 1977. *Solution of ill-posed problems*. John Wiley & Sons, New York.

Trushkin, D.V., Shushakov, O.A., and Legchenko, A.V. 1994. The potential of a noise-reducing antenna for surface NMR ground water surveys in the Earth's magnetic field. *Geophysical Prospecting* 42, 855-862.

Valla, P. and Legchenko, A. 2002. One-dimentional modelling for proton magnetic resonance sounding measurements over an electrically conductive medium. *Journal of Applied Geophysics* 50, 217-229.

Yaramanci, U. and Hertrich, M. 2007. Inversion of Magnetic Resonance Sounding data. *Boletín Geológico y Minero,* 118(3), 473-488.

Recibido: noviembre 2006
Aceptado: abril 2007